Applied Catalysis B: Environmental 90 (2009) 507–515

Contents lists available at ScienceDirect

Applied Catalysis B: Environmental

journal homepage: www.elsevier.com/locate/apcatb

Comparative heterogeneous contacting efficiency in fixed bed reactors: Opportunities for new microstructured systems

Ranjeeth R. Kalluri, Donald R. Cahela, Bruce J. Tatarchuk *

Center for Microfibrous Materials Manufacturing (CM³), Department of Chemical Engineering, Auburn University, 212 Ross Hall, Auburn, AL 36849, USA

ARTICLE INFO

Article history:
Received 10 July 2008
Received in revised form 8 April 2009
Accepted 8 April 2009
Available online 17 April 2009

Keywords:
Microfibrous
Monolith
Ozone
Heterogeneous
Reactor

ABSTRACT

Novel microstructured heterogeneous contacting systems called microfibrous entrapped catalysts (MFEC) were prepared by entrapping small particles of γ-alumina (150–180 μm) in sinter-locked network of metal (SS-304) microfibers (8 and 12 μm). These materials are in the form of thin flexible sheets (0.5–2.0 mm) and have uniform structures of high and variable voidages. Head-to-head theoretical comparisons of the performance efficiencies of flow-through pleated MFEC structures of various pleat factors (*PF* = face area of MFEC/cross-sectional area of the reactor) were made with packed bed reactors of various particle sizes (0.16–2.0 mm) and monolith reactors of various cpsi (100–900 cells per square inch). These comparisons showed that while packed beds produced high pressure drops, monoliths resulted in low fluid-solid mass transfer rates. On the other hand, MFEC structures with high *PF* (≥4) showed remarkable improvements in terms of conversion along with significant reduction in pressure drops and catalyst requirements compared to monoliths and packed beds. While small particles used in MFEC improved interphase and intraparticle mass transport rates, high voidages and ease of pleating helped lower the pressure drops in MFEC. To further ascertain these results, pleated structures of MFEC containing Pd/γ-alumina were tested for application in catalytic aircraft cabin air purification (ozone decomposition). Pressure drop and ozone conversion efficiency of pleated MFEC designs were measured at various flow rates and temperatures, and compared with those of a commercial monolith based ozone catalytic converter. The experimental results substantiated the mathematical findings.

1. Introduction

1.1. Background

Microfibrous entrapped catalysts (MFEC) and sorbents are a new class of microstructured materials [1–3] which have shown significant benefits in various heterogeneous catalysis and adsorption applications. Microfibrous entrapped ZnO/silica adsorbent beds have shown remarkable improvement in breakthrough times over packed beds in desulfurization of hydrogen reformate streams [4–6]. Substantial improvements in conversion and selectivity have been reported with use of MFEC for preferential catalytic oxidation of CO in hydrogen reformate streams and low temperature oxidation of CO in air [7,8]. Also, microfibrous entrapped activated carbon beds have shown significant benefits for VOC adsorption in various personal and collective protection applications [9,10]. MFEC have smaller characteristic dimensions and remarkably different internal structures compared to conventional contacting systems. These distinct characteristics of MFEC lead to higher reaction rates and lower pressure drops.

In this study, catalytic ozone decomposition for aircraft cabin air purification was used to demonstrate and understand the advantages of pleated MFEC structures. Monoliths are used in the commercial aircraft ozone converters and other air purification applications [11] mainly due to their lower pressure drops. Pleated MFEC are known to reduce pressure drops significantly [10]; hence, they were used in this study to design a more efficient catalytic air purification system. Theoretical comparisons of packed beds of various particle sizes, monoliths of various cpsi (cells per square inch) and MFEC with various pleat factors were made to see the effect of various reactor geometries on the pressure drop and reaction rate. An overall efficiency factor (χ), which combined both the above criteria, was used to evaluate the performance of the various reactor geometries. The effectiveness of each of the reactor systems in removing ozone was studied. Experimental ozone conversion and pressure drop tests were also conducted to verify the theoretical findings. However, the experimental comparisons were restricted only to monoliths

* Corresponding author at: 316 Ross Hall, Auburn University, Auburn, AL 36849, USA. Tel.: +1 334 844 2023; fax: +1 334 844 2063.
E-mail addresses: kallura@auburn.edu (R.R. Kalluri), caheldr@auburn.edu (D.R. Cahela), tatarbj@auburn.edu (B.J. Tatarchuk).

0926-3373/$ – see front matter © 2009 Elsevier B.V. All rights reserved.
doi:10.1016/j.apcatb.2009.04.015

Nomenclature

a_i	external surface area per unit vol. of solid component i (1/m)
a_p	external surface area per unit vol. of particles (1/m)
a_c	external catalyst surface area per unit vol. of catalyst (1/m)
C_A	gas-phase concentration of reactant (mol/m^3)
C_{Ai}	inlet concentration of reactant (mol/m^3)
C_{As}	concentration of reactant at catalyst particle surface (mol/m^3)
C_{Ao}	outlet concentration of reactant (mol/m^3)
C_D	coefficient of drag for sphere in turbulent flow (=0.6)
C_{FD}	coefficient of form drag for sphere in turbulent flow, $C_D - C_f$
C_f	coefficient of friction for sphere in turbulent flow
D_M	molecular diffusivity (m^2/s)
D_e	effective diffusivity inside catalyst (m^2/s)
d_c	characteristic length of reactor (m)
d_i	diameter of component i (m)
d_{ch}	monolith channel width (m)
d_p	catalyst particle diameter (m)
E_A	activation energy of reaction (J/mol)
f	friction factor
Gz	Graetz number, $Re_{ch}Scd_{ch}/L$
k_{eff}	effective reaction rate per unit catalyst volume (1/s)
k_m	gas phase mass transfer coefficient (m/s)
k_r	surface reaction rate per unit weight of catalyst (m^3/g/s)
k_0	pre-exponential factor in Arrhenius equation (m^3/g/s)
L	length/thickness of reactor bed (m)
ΔP	pressure drop (Pa)
Pe	reactor Peclet number, $\upsilon_0 L/D_M$
PF	pleat factor
R	universal gas constant (J/mol/K)
Re	Reynolds number, $d_c\upsilon_0\rho/\mu$
Re_{ch}	Reynolds number based on monolith channel width, $d_{ch}\upsilon_0\rho/\mu$
Re_p	Reynolds number based on particle diameter, $\varphi_p d_p\upsilon_0\rho/\mu$
Sc	Schmidt number, $\mu/\rho D_M$
Sh	Sherwood number, $k_m\varphi_p d_p/D_M$
T	temperature (K)
t_w	catalyst washcoat thickness (m)
t_c	monolith wall thickness (m)
x	position along the reactor length (m)
x_{FD}	$\varepsilon_b{}^2/12(1-\varepsilon_b)$
x_i	vol. fraction of solid component i
x_c	vol. fraction of catalyst support in reactor

Greek letters

χ	overall efficiency of reactor
ε_b	bed void fraction
ε_p	intraparticle voidage
Φ	Thiele modulus
η	internal effectiveness factor
φ_i	sphericity of solid component i, $6/d_i a_i$
φ_p	sphericity of particles, $6/d_p a_p$
μ	gas viscosity (kg/m s)
θ	flow path angle inside microfibrous media
ρ	gas density (kg/m^3)
ρ_c	catalyst support density (kg/m^3)
τ_b	bed tortuosity, $1 + (1-\varepsilon_b)/2$
τ_p	particle tortuosity
υ_0	superficial gas velocity (m/s)

and MFEC due to the practical difficulties associated with construction and testing of packed beds with the existing apparatus and the operating conditions of this application.

1.2. Microfibrous entrapped catalysts (MFEC)

Fig. 1 shows a micrograph of 150–250 μm γ-Al_2O_3 entrapped in a 1:1 ratio of 4 and 8 μm (nominal diameter) stainless steel (SS-304) microfibers. MFEC typically consist of small catalyst particles (50–300 μm) entrapped in 2–20 μm microfibers. The choice of fiber material—polymer, ceramic or metal can be made depending upon requirements of the reaction/adsorption process under consideration. The relatively small catalyst particles used in MFEC result in higher heat and mass transport rates compared to conventional reactor systems with larger characteristic dimensions (particle sizes, channel widths, etc.).

MFEC are prepared in wet lay paper making process, which helps achieve high structural uniformity. This structural uniformity in MFEC helps minimize intrabed channeling or flow maldistributions [9]. The catalyst particles in MFEC are held in space by three-dimensional sinter-locked network of high aspect ratio (length to diameter ratio) microfibers. The typical volume loadings of catalyst and fibers in MFEC are about 10–25% and 1–5%, respectively, with the rest being void. The high voidages in MFEC help decrease the pressure drops in these systems significantly. Another benefit of MFEC is their flexibility for pleating, which helps achieve higher conversions and lower pressure drops. This aspect of MFEC will be explored in detail in this study.

1.3. Catalytic ozone decomposition and aircraft cabin air purification

Ozone is a key pollutant entering aircraft cabin air at cruising altitudes [11,12]. At altitudes of about 12 km above the sea level (typical cruising altitude of commercial jets) ozone concentrations

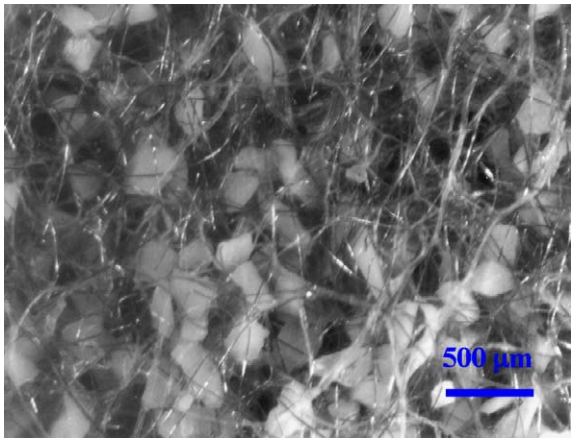

Fig. 1. Micrograph of 150–250 μm γ-Al_2O_3 entrapped in 4 and 8 μm (1:1 ratio) stainless steel microfibers.

as high as 6.0 ppmv can be found in the atmosphere [11,13]. While this naturally occurring ozone present at higher altitudes protects us from the harmful UV radiation of the Sun, it can cause severe health effects to the passengers and crew if it is not removed from the air entering the aircraft cabin. The Environmental Protection Agency (EPA) standards for ozone exposure limits are a time weighted average of 0.08 ppmv for an 8 h period and 0.12 ppmv for a 1 h period [13]. Exposure to higher concentrations of ozone can cause severe irritation in eyes, nose and throat, and several other respiratory illnesses [14,15].

Many industrial equipment like plasma generators, UV lamps, copiers, printers, etc. can also produce ozone in ppm levels at ground level. Ozone is widely used in many municipal water purification systems and also as a disinfectant in the food industry [16]. The excess unreacted ozone can become a potential pollutant. Hence, all these processes require an efficient ozone removal system to eliminate the possible health hazards of ozone.

Catalytic decomposition of ozone into diatomic oxygen is the most widely used method for ozone elimination. A detailed account of various catalysts used in the ozone decomposition reaction, their activities and rate mechanisms is given elsewhere [17–19]. Development of better or improved catalysts was beyond the scope of this work. As mentioned before, this research is focused on understanding the advantages of pleated MFEC structures as compared to the conventional reactors using a case study of catalytic ozone decomposition for aircraft cabin air purification. This application involves high gas flow rates and is quite demanding in terms of pressure drop as well as conversion. The surface reaction rate for the catalyst used in this study was very high; this enabled high ozone conversions even for very short gas residence times inside the reactors.

2. Mathematical models

Theoretical performance comparisons of MFEC were made with packed beds and monoliths for catalytic ozone decomposition application. The mathematical models used to represent the mass and momentum transfer rates in various reactor geometries and the performance evaluation criteria employed are presented in this section.

Although ozone decomposition is a highly exothermic reaction, due to the low ozone concentrations (Section 3.3) involved in this application, no appreciable temperature rise is expected in the reactor even for complete ozone conversion. Also the reactor *Pe* are sufficiently high (>10) owing to the high velocities under consideration. Therefore, isothermal plug flow conditions were assumed in this study. Pressure variations along the reactor length were neglected in the theoretical comparisons. The ideal gas law was used to estimate the density of gas stream. The operating conditions and some of the parameters used in these theoretical comparisons are shown in Table 1. The molecular diffusivity (D_m) of ozone in air was estimated using Fuller's method. The relevant equations and the parameters used in this calculation are described in detail by Reid et al. [20]. The viscosity value listed in the table corresponds to air at the operating conditions.

The pressure gradient in packed beds, monoliths or MFEC can be described by the following general equation, where f is a friction factor and d_c is the characteristic length, specific for each reactor type

$$\frac{-\Delta P}{L} = \left(\frac{2f}{d_c}\right)\rho v_0^2 \tag{1}$$

The characteristic length (d_c) for packed beds and MFEC is equal to the effective particle diameter ($\varphi_p d_p$) whereas for monoliths it is equal to the channel diameter (d_{ch}). The friction factors and gas–solid mass transfer coefficients (or *Sh*) for each of the reactor geometries were estimated using specific correlations discussed below.

Table 1
Operating conditions and parameters used in the theoretical comparisons.

Operating conditions	
Temperature (K)	394
Pressure (Pa)	1.01×10^5
Inlet ozone concentration (ppmv)	1.5
Parameters	
D_m ($m^2\ s^{-1}$)	2.90×10^{-5}
D_e ($m^2\ s^{-1}$)	8.73×10^{-6}
μ (kg/m s)	2.29×10^{-5}
k_0 (m^3/kg s)	8.35×10^4
E_A (kJ/mol)	21.08

2.1. Packed beds

The various packed bed particle diameters compared in this study along with bed properties used are listed in Table 2. The smallest particle size used in packed beds matches with the MFEC catalyst particles (Section 2.3). This enables a direct comparison of packed beds and MFEC performances. Friction factors for packed beds were estimated using Ergun equation:

$$2f = \left(150\left(\frac{1-\varepsilon_b}{Re_p}\right) + 1.75\right)\left(\frac{1-\varepsilon_b}{\varepsilon_b^3}\right) \tag{2}$$

The *Sh* for packed beds were obtained using Thoenes–Kramers correlation [21]:

$$Sh = \frac{(1-\varepsilon_b)^{1/2}}{\varepsilon_b} Re_p^{1/2} Sc^{1/3} \tag{3}$$

It is a semi-empirical correlation widely used for predicting the mass transfer coefficients in packed beds with $40 < Re_p/(1-\varepsilon_b) < 4000$ and $0.25 < \varepsilon_b < 0.5$ [21]. The Re_p and bed voidage for packed bed cases used in this study are within these limits. The intraparticle transport rates in packed beds were modeled using the following effectiveness factor equations [21]:

$$\eta = \frac{1}{\Phi}(\coth(3\Phi) - 1/3\Phi) \tag{4}$$

where

$$\Phi = \left(\frac{\varphi_p d_p}{6}\right)\sqrt{\frac{k_r \rho_c}{D_e}} \tag{5}$$

For all the reactor geometries compared, the effective diffusivity (D_e) of the ozone inside the catalyst support was obtained using Eq. (6), with $\tau_p = 2.5$ and $\varepsilon_p = 0.75$. These values of intraparticle tortuosity and porosity correspond to the γ-alumina used in the experiments (Section 3.1).

$$D_e = D_m \frac{\varepsilon_p}{\tau_p} \tag{6}$$

2.2. Monoliths

The various monolith cases compared in this study along with their structural properties are listed in Table 3. These values of wall thicknesses and cell densities are the most widely used commercial ceramic monolith variations [22–24]. The catalyst washcoat

Table 2
Packed bed particle diameters and bed properties used in the theoretical comparisons.

Particle diameters, d_p (mm)	0.16, 0.5 and 2.0
Sphericity (φ_p)	0.7
Void (vol.%)	40
Catalyst (vol.%)	60

Table 3
Properties of various monoliths used in the theoretical comparisons.

Cells per square inch (cpsi)	100	400	900
Wall thickness, t_w (0.001 in./μm)	15/381	6.5/152	2/51
Catalyst washcoat thickness, t_c (μm)	25	25	25
Channel dia., d_{ch} (mm)	2.109	1.068	0.745
Void (vol.%)	68.94	70.67	77.56
Catalyst (vol.%)	3.31	6.77	10.75
Length, L (cm)	12.7	12.7	12.7

thickness in monoliths is generally kept to a minimum to minimize the pore diffusion resistances. In typical commercial monoliths it is about 20 and 60 μm on the wall surfaces and the corners, respectively [11]. Due to the accumulation of washcoat near the corners of the channels, the effective catalyst washcoat thickness is greater than that on the channel walls. Therefore, a value of 25 μm was used in this study to represent the average washcoat thickness. A whole range of other variations of cpsi, wall thicknesses and washcoat thicknesses could be considered but this study was aimed at comparing MFEC with the commercially available monolith variations, assuming their dimensions are optimized from a practical stand point. Only square channel monoliths were considered here; any other channel shape is expected to show trends similar to that observed in this study.

The friction factors for monoliths were estimated using the following correlations [11]:

$$f = \frac{13}{\varepsilon_b Re_{\mathrm{ch}}} \quad \text{for } \frac{Re_{ch}}{\varepsilon_b} < 1000$$
$$= \frac{0.03}{\varepsilon_b^{1.88} Re_{\mathrm{ch}}^{0.12}} \quad \text{for } \frac{Re_{ch}}{\varepsilon_b} > 1000$$

There are many empirical correlations and theoretical equations available in literature [25–27] for predicting the fluid-phase mass transfer coefficients for monoliths. In this study the correlation (Eq. (8)) proposed by Tronconi and Forzartti [25] for the mass transfer in square channel monoliths was employed.

$$Sh = 2.967 + 8.827 \times \left(\frac{1000}{Gz}\right)^{-0.545} \exp\left(\frac{-48.2}{Gz}\right) \tag{8}$$

The internal effectiveness factors for monoliths were calculated using Eqs. (9) and (10). For the theoretical comparisons, the catalyst washcoat density was assumed to be the same as that of particle density of alumina support.

$$\eta = \frac{\tanh(\Phi)}{\Phi} \tag{9}$$

where

$$\Phi = t_c \sqrt{\frac{k_r \rho_c}{D_e}} \tag{10}$$

2.3. MFEC

The bed properties and pleat factors of MFEC structures used in the theoretical comparisons are listed in Table 4. These values of bed properties match those of the experimentally tested structure which will be described further in Section 3.1. Fibers in MFEC resemble infinitely long cylinders with ridges on the surface. The shape factor for an infinitely long cylinder is 1.5. This was multiplied by a factor of 0.7 to account for the surface roughness due to the ridges on the fibers. Fig. 2 shows sketches of plain and pleated MFEC reactor designs. Pleat factor (*PF*), a term frequently used with MFEC systems, is defined as follows:

Table 4
MFEC cases and bed properties used in the theoretical and experimental comparisons.

PF	1, 2 and 4
Particle diameter, d_p (mm)	0.16
Nominal fiber diameter (μm)	8 and 12 (1:1 wt. ratio)
Catalyst particle sphericity (φ_p)	0.7
Fiber sphericity (φ_i)	1.05 (=1.5 × 0.7)
Catalyst (vol.%)	13.6
Metal (vol.%)	1.2
Void (vol.%)	85.2

$$\mathrm{PF} = \frac{(\text{total face area of MFEC media})}{(\text{cross-sectional area of the reactor})} \tag{11}$$

PF values for monoliths and packed beds are always equal to one, as they cannot be pleated. For estimating the friction factors in MFEC systems the porous-media permeability equation proposed by Cahela and Tatarchuk [28,29] was used:

$$2f = \left\{72\left[\left(\sum \frac{x_i \varphi_p d_p}{\varphi_i d_i}\right)^2 + x_{FD} \sum x_i \left(\frac{\varphi_p d_p}{\varphi_i d_i}\right)^2\right] \frac{(1-\varepsilon_b)}{PF\, Re_p} + 3\frac{\tau_b}{\cos(\theta)} \frac{1}{PF^2}\left[C_f + C_{FD}\frac{\varepsilon_b}{4}\right] \sum\left(\frac{x_i \varphi_p d_p}{\varphi_i d_i}\right)\right\} \frac{(1-\varepsilon_b)}{\varepsilon_b^3} \frac{\tau_b^2}{\cos^2(\theta)} \tag{12}$$

This equation can be used to predict the pressure drops in multiparticulate beds with voidages as high as 0.99 and its applicability for MFEC structures has been verified by the authors [28–30]. A detailed derivation of the above equation (except for the '*PF*' correction) and the significance of each of the above terms are also given in the above mentioned references. The term '*PF*' in the above equation was introduced as part of this work. This inclusion only accounts for the decreased gas velocity (due to pleating) inside the MFEC media. It does not account for the pressure losses due to the change in velocity magnitude and direction (flow comes in at an angle to the media surface) at the entrance and the exit of the pleated MFEC media. The extent of these inertial losses and

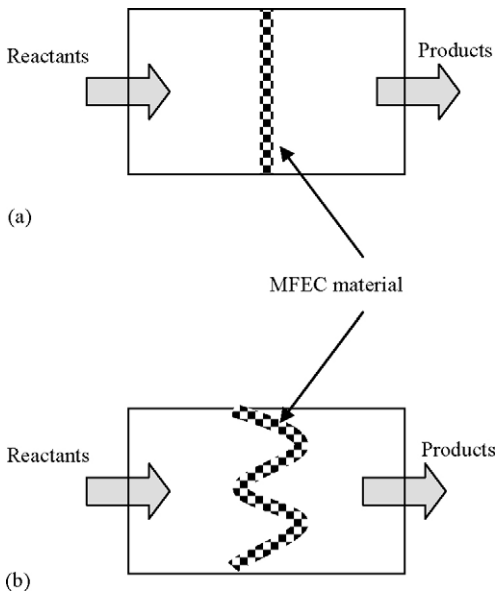

Fig. 2. Schematic of MFEC reactors. (a) Plain design (*PF* = 1) and (b) pleated design (*PF* > 1).

their impact on the reactor performance comparisons will be discussed further in the results section (Section 4.1).

To predict the *Sh* in MFEC, the following empirical equation proposed by Dwivedi and Upadhyay [31] for gas–solid contacting in fixed beds was used:

$$Sh = \frac{0.455}{\varepsilon_b}\left(\frac{Re_p}{PF}\right)^{0.59} Sc^{0.33} \tag{13}$$

This correlation was chosen for MFEC as it was obtained by correlating a wide range of literature data of fixed bed gas–solid contacting systems with bed voidages ranging from 0.25 to 0.97 and Re_p from 1 to 10000. The voidage term in the above equation was introduced after a comprehensive review of fixed bed mass transfer literature [31]. The *PF* correction in the above equation was introduced as a part of this study to correct for the actual velocity inside the MFEC bed. Thoenes–Kramers correlation, used for packed beds, is not suitable for high voidage MFEC structures. Eq. (13) could also be used for packed beds, in which case the mass transfer coefficients could differ (up to 20%) from the values obtained using Thoenes–Kramers correlation (for packed bed Re_p). However, this difference in predicted mass transfer coefficients for packed beds, does not significantly affect the comparative analysis or trends obtained in this study (Section 4.1).

The fibers in MFEC can help distribute the fluid flow between the particles; hence they can positively influence the mass transfer rates. The Re_p for the cases with $PF = 4$, which will be of greater interest in this study (Section 4), are less than 40. Based on a different study [30] made by the present authors utilizing computational fluid dynamics (CFD) simulations, the increase in mass transfer rates due to fibers in channel geometries was estimated to be up to 30% for the $Re < 40$ and *Sc* of present study. This increase is expected to be lower for the case of catalyst particles entrapped in fibers (like MFEC). A more detailed analysis of the effect of fibers on mass transfer rates in MFEC is beyond the scope of the present study. In this study, for simplicity of calculations the presence of fibers was neglected in the mass transfer estimations (except for the bed voidage calculations) of MFEC. If included this could further increase the mass transfer rates and overall efficiency factors (Section 2.4) for MFEC cases. However, the performance trends observed with respect to the change in *PF* (Section 4.1) are expected to remain the same. Lastly, the internal effectiveness factors for MFEC were calculated using similar equations as that of the packed beds described before.

2.4. Performance evaluation criteria

The gas phase differential mass balance for reactant A in any plug flow reactor is given by the equation:

$$-\frac{\upsilon_0}{PF}\frac{dC_A}{dx} = k_m a_c x_c (C_A - C_{AS}) \tag{14}$$

The gas–solid mass transfer rate in above expression should also be equal to the reaction rate inside the catalyst. Assuming a first order surface kinetics:

$$k_m a_c x_c (C_A - C_{As}) = \eta k_r \rho_c x_c C_{AS} \tag{15}$$

If k_{eff} is the effective reaction rate constant per unit volume of catalyst, then we can also write (similar to Eq. (15))

$$-\frac{\upsilon_0}{PF}\frac{dC_A}{dx} = k_{eff} x_c C_A \tag{16}$$

Eliminating the concentration terms from Eqs. (14)–(16) gives

$$\frac{1}{k_{eff}} = \frac{1}{k_m a_c} + \frac{1}{\eta k_r \rho_c} \tag{17}$$

The performance comparison of different reactor geometries was made using a methodology similar to that described in some earlier studies [32–34]. Overall efficiency factor (χ), a ratio which combines pressure drop and conversion (reaction rate) into a single parameter was defined as follows

$$\chi = \frac{\ln(C_{Ai}/C_{Ao})_{Max}}{(-\Delta P/\rho \upsilon_0^2)}. \tag{18}$$

The subscript '*Max*' in the above expression indicates the maximum attainable conversion in a given reactor geometry under a given set of operating conditions. For a first order kinetics, this occurs when the reactor is operated in a complete gas–solid mass transfer controlled regime [27], i.e., $C_{AS} = 0$. Integrating Eq. (14) with $C_{AS} = 0$ results in

$$\ln\left(\frac{C_{Ai}}{C_{Ao}}\right)_{Max} = k_m a_c x_c \left(\frac{L}{\upsilon_0/PF}\right) \tag{19}$$

Substituting for pressure drop and log reduction in Eq. (18) from Eqs. (1) and (19), respectively, gives

$$\chi = \frac{k_m a_c x_c d_c PF}{2 f \upsilon_0} = \frac{Sh\, a_c d_c x_c\, PF}{2\, fReSc} \tag{20}$$

Evidently, the higher the χ value the better the performance, as it gives higher conversion with lower pressure drop.

2.5. Surface kinetics

For the catalyst used in the experimental study (Section 3.1), the ozone decomposition kinetics follow a first order rate law [19]. Therefore, a first order rate expression was used to model the surface reaction rate. An Arrhenius plot of the ozone decomposition kinetics for the catalyst used in this study is shown in Fig. 3. The surface reaction rate constants (k_r) were back-calculated from the experimental MFEC ozone conversion data (Section 4.2). This was done by iteratively solving Eqs. ((4), (5) and (17)) with volumetric reaction rate constants (k_{eff}) obtained from ozone conversion measurements and gas–solid mass transfer constants (k_m) estimated from Eq. (13). The parameters for Arrhenius equation (Eq. (21)) were obtained by fitting a straight line through these data points.

$$k_r = k_0 \exp\left(\frac{-E_A}{RT}\right) \tag{21}$$

The values of pre-exponential factor and activation energy in the above equation are listed in Table 1. These values were used to compute the surface reaction rates in the theoretical calculations for all the reactor geometries.

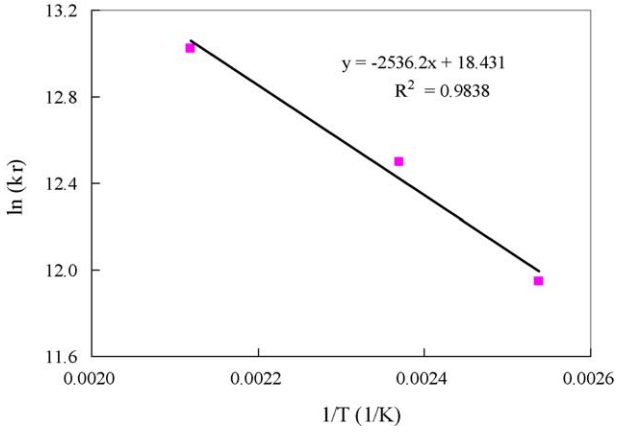

Fig. 3. Arrhenius plot for catalytic ozone decomposition reaction for Pd/γ-alumina.

Table 5
Properties of γ-alumina used in experiments.

Particle density, ρ_c (kg/m^3)	1210
Particle void fraction, ε_p	0.75
Surface area (m^2/g)	220

3. Experimental details

3.1. Preparation of MFEC

γ-Alumina was obtained from Alfa Aesar in the form of 3.2 mm cylindrical extrudates and was sized to (150–180 μm) particles. Properties of γ-alumina obtained from its product data sheet are mentioned in Table 5. Traditional paper-making technique was used to prepare microfibrous composite materials. In this process, an aqueous suspension consisting of 8 g each of 8 and 12 μm nominal diameter (1:1 weight ratio) metal (SS 304, Intramicron Inc.) fibers, 10 g of cellulose and 35 g of γ-alumina (150–180 μm) particles was formed by rapid stirring. The resulting suspension was then transferred into the head box of a paper making equipment (MK sheet former) and the excess water was drained to form uniform (1 sq.ft) square sheet of microfibrous entrapped alumina. Multiple sheets were prepared in this manner and these sheets were dried at 373 K for 15 min and subsequently oxidized in air at 673 K for 1 h to remove cellulose, before being sintered at 1323 K for 30 min in H_2. The resulting MFEC sheets were about 1 mm thick and had properties as mentioned in Table 4. The γ-alumina particles in MFEC were then impregnated using incipient wetness technique with palladium tetraamine acetate. Pd was used, as it is widely used in commercial monolith based aircraft ozone catalytic converters [24,35,36]. Finally, the impregnated MFEC samples were dried (373 K) and calcined (723 K). MFEC sheets with 1.0% Pd/γ-Al_2O_3 were thus prepared. These sheets were stacked to obtain a required bed thickness of about 4 mm, then they were cut to required shapes and later used in building the pleated structure (PF = 4) shown in Fig. 4. This whole unit was about 14 cm in diameter and 35 cm in length. The above MFEC sheets were also used in a PF = 1 design for some pressure drop measurements.

3.2. Commercial monolith based catalytic converter

The performance of MFEC was compared with a commercial monolith based ozone catalytic converters (BASF P/N: D19333-5, 20499004). The pressure drops and conversions for these commercial converters were obtained from their product data sheet [37] and the data was available only for one set of operating conditions each.

3.3. Experimental setup

The ozone converter test setup consisted of a high pressure blower (Fan Equipment Company Inc.) circulating air inside a closed-loop system as shown in Fig. 5. A variable speed drive (not shown in figure) was used to change the gas flow rate inside the system. The energy dissipated by the blower also heated the air inside the loop. A fraction of this gas stream was continuously purged to control the temperature of the system. Ozone was generated by passing air through a PZ2-12 ozone generator obtained from Prozone Water Products, Intl. The generated ozone was then mixed with a bulk air stream from the blower to obtain a required concentration (1.5 ppmv) of ozone at the inlet of the ozone converter. A Eco Sensors UV-100 ozone analyzer was used to measure the ozone concentration at the inlet and outlet of the ozone converter. The entire system was operated at close to atmospheric pressure. The pressure drop across the converter was measured and recorded for various inlet conditions. Temperatures at the inlet of the catalytic converter were measured with a K-type thermo couple (Omega). The experiments on MFEC were conducted at three different temperatures—394 K, 422 K and 472 K. The range of the gas velocities and temperatures used in these tests include the conditions employed in commercial aircraft cabin air purification systems [37].

4. Results and discussion

4.1. Theoretical comparisons

Fig. 6 shows a plot of volumetric mass transfer coefficients ($k_m a_c$) versus superficial velocity for various reactor geometries listed in Section 2. As discussed before, $k_m a_c$ is the maximum attainable reaction rate constant for a given reactor geometry and operating conditions. As evident from the plot, volumetric mass transfer coefficients in monoliths are significantly lower than that of the smaller particle packed beds and MFEC. This underscores one of the major disadvantages associated with monoliths, namely, the low gas–solid mass transfer rates. The $k_m a_c$ values in the

Fig. 4. MFEC ozone converter with PF = 4.0.

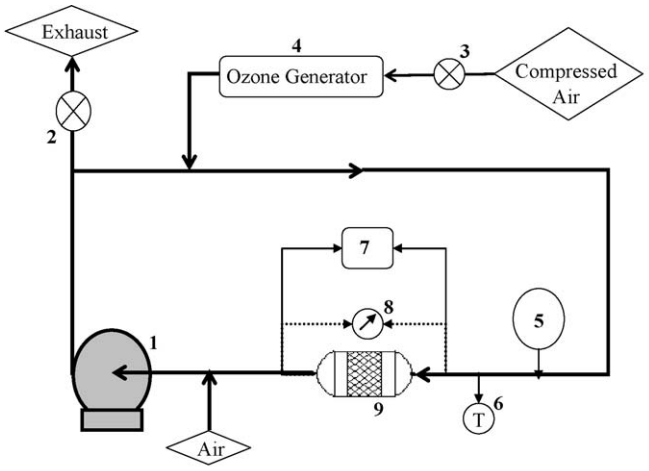

1. High pressure blower; 2. Valve 3. Mass flow controller; 4. Ozone generator; 5. Flow meter (pitot tube); 6. Thermometer; 7. Ozone meter; 8. Pressure drop measurements; 9. MFEC catalytic converter.

Fig. 5. Schematic of ozone catalytic converter test setup.

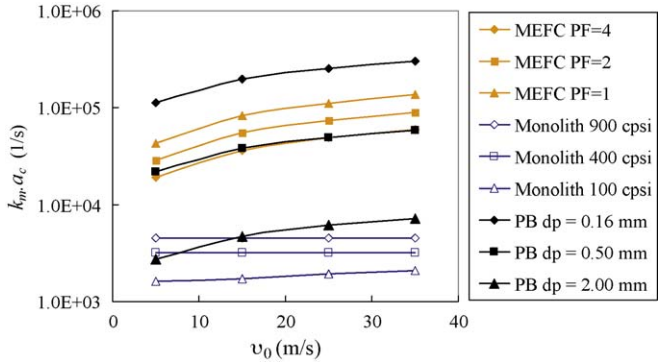

Fig. 6. Volumetric mass transfer coefficients ($k_m a_c$) versus superficial velocity for different reactor geometries.

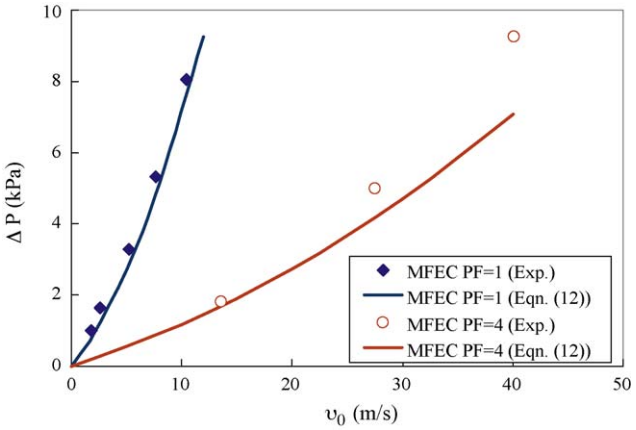

Fig. 8. Comparisons of model versus experimental pressure drop measurements for MFEC structures with different *PF*.

packed beds increased dramatically with decrease in particle size, benefiting from the increase in particle surface area. Although all the cases of MFEC had same particle diameter and bed composition, the mass transfer coefficients decreased with increasing *PF*. This is a result of decrease in the effective velocity inside the MFEC structures with increase in *PF*. Also, the mass transfer coefficients for the MFEC were found to be lower than that of the packed beds with the same particle size (0.16 mm). This is due to the higher voidage of MFEC structures compared to the packed beds, which negatively affects the gas–solid mass transfer coefficients.

Fig. 7 shows the comparisons of overall efficiency factors (χ) versus superficial velocity for the various reactor geometries. Evidently, the χ values of the packed beds compared poorly with respect to that of the monoliths. This is in spite of the higher gas–solid mass transfer rates observed in small particle packed beds and it is a direct result of significantly higher pressure drops in packed beds compared to monolith channels. This underscores the major advantage of monoliths over packed beds and explains the reason behind their wide usage in various catalytic applications. There is a slight increase in the χ values with decreasing particle size in packed beds. Similarly, the χ values for monoliths also improved slightly with increasing cell density (decreasing channel width). But, these internal variations in χ values in both packed beds and monoliths are relatively narrow.

The χ values of MFEC with *PF* = 1, although slightly better than that of the packed beds, were found to be significantly lower than that in monolith reactors. MFEC with lower *PF* tends to exhibit more are less the same characteristics as the small particle packed beds. But the overall efficiency of MFEC systems improved dramatically with increase in *PF*. As shown in the plot, the χ value for MFEC at *PF* = 4.0 is significantly better than that of monoliths. With increase in *PF*, the effective velocities in MFEC were cut down by an equivalent factor and the pressure drops decreased accordingly. For the same reason, the residence times as well as the associated conversions increased with increase in *PF*. This clearly shows that the high *PF* MFEC designs can provide higher conversions with lower pressure drops.

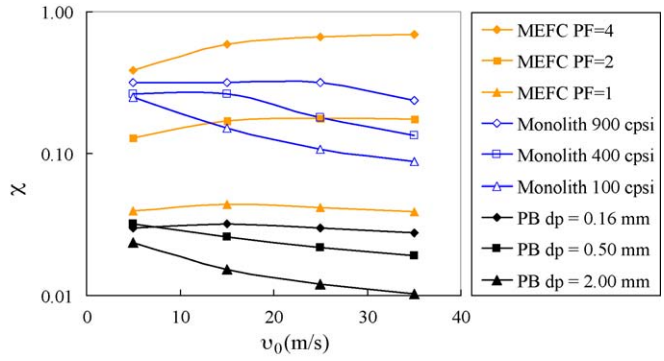

Fig. 7. χ versus superficial velocity for different reactor geometries.

Fig. 8 shows comparisons of the model (Eq. (12)) based and the experimental pressure drops at 472 K for the present *PF* = 1 and *PF* = 4 MFEC designs (Section 3.1). The model predictions are in reasonable agreement with experimental values for *PF* = 1. For *PF* = 4, the experimental values are (up to 30%) greater than that of the model predictions. This difference can be attributed to the inertial pressure losses (due to change in velocity magnitude and direction) at the entrance and exit of the pleated MFEC media. As discussed before, these pressure losses are not accounted by the *PF* correction in Eq. (12). These inertial losses are expected to increase proportionately with the square of fluid velocity. This explains the increase in the difference between the model and experimental pressure drop values for *PF* = 4 design with increase in velocity. A given *PF* value can be achieved using multiple MFEC designs. While the pressure losses inside a given MFEC media are dependent only on *PF*, the extent of the above discussed inertial losses also depend on the actual design (number of pleats, pleat depth, etc.) of the pleated MFEC reactor. Also, these inertial losses are more or less constant for a given MFEC design (for a small *L*), and unlike the pressure losses inside the MFEC media, they do not increase proportionately with increasing MFEC bed thickness. Hence, to keep the results (χ values) independent of the MFEC bed thickness and design, they were not included in the χ and *f* definitions.

These inertial pressure losses if included can reduce the χ values for MFEC reactors for *PF* greater than one. However, for the present operating conditions and *PF* = 4 design (basing on Figs. 7 and 8), the MFEC χ values will remain higher than the monolith χ values even if the above pressure losses are included. The *PF* for MFEC can be raised further (>4), but with further increase in pleating these inertial losses are expected to increase drastically, which could in turn negate the advantages of pleating. Further, the curvature in velocity stream lines (change in velocity direction) at the entrance and exit can also improve the mass transfer coefficients in MFEC similar to that of the inertial pressure losses. These gains in mass transfer rates in MFEC can at least partially compensate the decrease in χ values due to the inertial pressure losses discussed above.

Balakotaiah and West [38] give a detailed theoretical analysis of mass transfer and pressure drop in convex geometries (such as circle, square, triangle, etc. shaped monolith channels), and they also present a simple criteria (based on '*f Re/Sh*', similar to the Eq. (20)) for optimal design of catalytic monoliths and packed beds operating in the interphase mass transfer controlled regime. With

the help of this criteria, they further conclude that the creation of a transverse velocity component due to variation in bed cross-sectional area and connectedness of channels, improves the momentum as well as mass transport rates, and there exists an optimum *Re* for a given reactor geometry at which the highest χ value (maximum mass transfer rate for a given pressure drop) is achieved. These optimum *Re* values for various reactors (in Fig. 7) can be found easily by plotting χ versus *Re*. In this study, χ values for various reactors were plotted against inlet velocity to compare the reactor performances at the same inlet conditions (which are of interest for the present application).

Similar to the optimum in *Re*, one can expect that there exists an optimum *PF* and pleat geometry of MFEC reactors at which the highest χ values can be obtained. A more detailed analysis of the above mentioned mass transfer gains and inertial pressure losses with increasing *PF*, and estimation of the optimum *PF* values for MFEC reactors are beyond the scope of the present study and will be considered in our future work.

The above discussion and plots regarding χ and $k_m a_c$ are generic and not specific to any specific surface reaction rates. Fig. 9 shows the variation of effective volumetric reaction rates in different reactor geometries for the ozone decomposition reaction on the catalyst used in this study. Effective reaction rate per unit catalyst volume (k_{eff}) is a measure of the extent of catalyst utilization in the reactor. The effective reaction rates, to some extent, reflect the trends seen in $k_m a_c$ plot as the surface kinetics involved are very fast. The internal effectiveness factor for all the monoliths used in this theoretical study was a constant ($\eta = 0.29$) as the catalyst washcoat thickness was fixed ($t_c = 25\ \mu m$) for all the cases. Although this effectiveness factor for the monoliths is close to that of all the MFEC reactors and the packed bed with $d_p = 0.16$ mm ($\eta = 0.34$), the volumetric effective reaction rates in monoliths are remarkably lower than that of the other reactors. These low reaction rates in monoliths imply poor utilization of the catalyst.

The results shown above also indicate that the MFEC and small particle packed beds tend to benefit the most from high catalyst activity (high surface reaction rates). This is because the monoliths and large particle packed beds were found to be significantly gas–solid mass transfer limited; therefore their performance would not improve significantly with increase in surface reaction rates.

In this study, the comparisons of MFEC were restricted only to packed beds and monoliths. Using the same definition for χ as that used in this study, Giani et al. [33] have shown that the χ values for catalytic foams lie between 0.1 and 0.3 for a wide range of *Re*. Basing on these values and the results in Fig. 7, it can be concluded that while MFEC *PF* = 1 may not be as good as catalytic foams, MFEC designs with $PF > 2$ can perform better than catalytic foams also.

The construction and operation of the packed bed cases considered in this theoretical study, especially the smaller particle

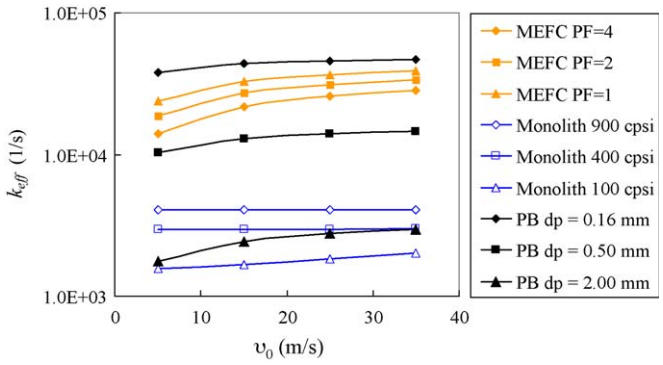

Fig. 9. Effective reaction rate constants versus superficial velocities for different reactor geometries.

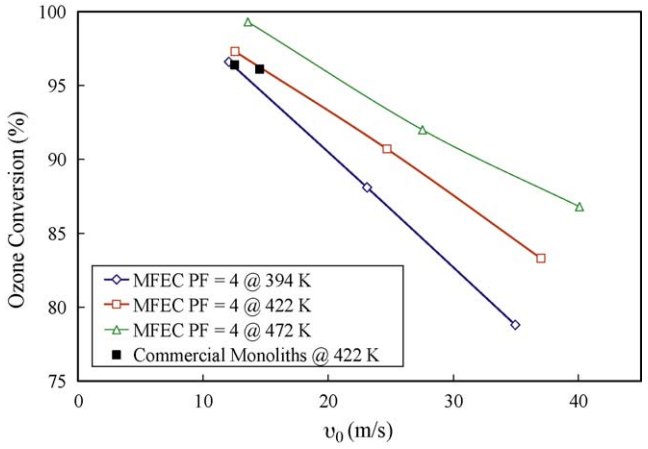

Fig. 10. Experimental conversion comparisons of MFEC (*PF* = 4.0) with commercial monoliths converters.

cases, may not be feasible in practice for the operating conditions (velocities used and mobile settings) of this application, as this would require construction of extremely (<5 mm) thin packed beds in order to keep the pressure drops sufficiently low. But those cases were included in the theoretical study to make a comprehensive comparative study of MFEC with the major conventional fixed bed reactors.

There are many mass transfer and pressure drop correlations available in the literature for different fixed bed types and operating conditions. The choice of the correlations used in this study was based on the operating conditions and corresponding *Re* and *Sc* ranges of the present application. A different choice of these correlations for any of the various contacting systems (bed type) considered in this study, might slightly change the actual χ values, but would not significantly alter the χ value trends obtained in this study.

4.2. Experimental comparisons of monoliths and MFEC

The experimental ozone conversion and pressure drop comparisons of MFEC *PF* = 4.0 design and commercial monolith ozone converter described before (Section 3.2) are shown in Figs. 10 and 11, respectively. As mentioned before, limited data points were available for the commercial monolith converters [37]. Conversion in the MFEC reactor was slightly better than that of the commercial monolith systems. The pressure drop in monoliths was significantly higher than that in the MFEC for similar flow conditions. This implies the overall efficiency factor for the *PF* = 4.0 MFEC

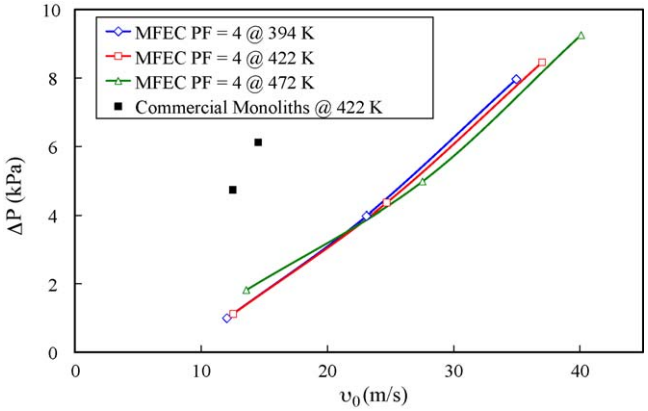

Fig. 11. Experimental pressure drop comparisons of MFEC (*PF* = 4.0) with commercial monoliths converters.

design is higher than that of the monolith converter. This was expected from the theoretical results in Fig. 7. The exact catalyst composition and loading in the commercial monolith converter under consideration is not known. However, as the commercial monoliths are almost always operated in interphase mass transfer controlled regime (to maximize their performance [11,27]), the actual surface reaction rate (or the catalyst type and/or loading) is not of a major significance.

Further, in the above experiments (Fig. 10), MFEC reactor operation was not completely in the interphase mass transfer controlled regime, and hence, there is further scope for improving the reactant conversion in MFEC by increasing the catalytic activity. However, as interphase mass transfer is the rate controlling step in monolith reactors, the experimental conversion data for monoliths represents the maximum attainable values for the given temperature and monolith geometry. Therefore, it can be safely concluded that a higher catalyst activity and/or a higher temperature will significantly benefit the MFEC reactors while leaving the monolith performance more or less unaffected.

Further, the experimental temperatures in this study were chosen so as to match the operational range of the commercial aircraft cabin air purification application. Also, higher temperatures could not be used in these experiments due to the (safe operability) limitations in the design of the present test apparatus. The bed composition and/or properties (*PF*, voidages, catalyst loading, particle and fiber diameters, etc.) of MFEC structure used in these experimental and theoretical comparisons also requires further optimization. As the bed properties of microfibrous materials can be easily tailored to the requirements of specific applications, our future work will be focused on MFEC optimization and operation in interphase mass transfer regime in order to derive their full benefit.

5. Conclusions

The overall contacting efficiencies of packed beds, irrespective of the particle sizes used, were found to be lower than that of the monoliths and MFEC. While the packed beds of larger particles offered less resistance to flow (low pressure drops), they were mainly constrained by the (interphase and intraparticle) mass transport resistances. The packed beds of smaller particles, on the other hand, had high mass transfer rates but the associated pressure drops were also high. Therefore, the packed beds were found to be relatively inefficient in terms of the contacting efficiency. Monoliths offer low resistance to flow (or low pressure drop) due to straight channels and also low pore diffusion resistances due to thin catalyst coatings. Hence, they have higher overall efficiencies compared to packed beds and MFEC with low *PF*. The limitation in monoliths mainly comes in the form of lower interphase mass transfer coefficients compared to packed beds and MFEC.

Although the overall contacting efficiency of MFEC with lower *PF* was less than that of the monoliths, it improved drastically with increase in *PF*. This increase in χ in MFEC was a direct result of a proportionate decrease in the effective velocity (inside MFEC media) associated with increase in *PF*. The decreased effective velocity results in lower pressure drops and also higher residence time or, in other words, higher conversion. This dual advantage achieved with pleating MFEC media leads to higher χ values in MFEC compared to that of monoliths. Also as the effective reaction rates in MFEC were higher than that of the monoliths, MFEC structures are more optimized compared to monoliths in terms of catalyst utilization. While small particles used in MFEC lead to high interphase and intraparticle transport rates, high voidages and ease of pleating result in low pressure drops.

Experimental conversion and pressure drop measurements of MFEC structure with $PF = 4.0$ compared better than that of a commercial monolithic converter. These results further established the theoretical findings. MFEC with higher *PF* have demonstrated better overall efficiencies – lower pressure drops and better effective reaction rates (catalyst utilizations) – compared to the conventional reactor systems. As this study showed some remarkable advantages of MFEC, further optimization of MFEC bed composition seems very promising.

Acknowledgment

This work was funded in part by U.S. Army Tank-Automotive Research, Development and Engineering Center (TARDEC), under contract ARMY-W56HZV-05-C-0686.

References

[1] B.J. Tatarchuk, M.R. Rose, A. Krishnagopalan, J.N. Zabasajja, D. Kohler, US Patent 5,080,963 (1992).
[2] B.J. Tatarchuk, M.F. Rose, A. Krishnagopalan, US Patent 5,102,745 (1992).
[3] B.J. Tatarchuk, M.F. Rose, G.A. Krishnagopalan, J.N. Zabasajja, D.A. Kohler, US Patent 5,304,330 (1994).
[4] Y. Lu, N. Sathitsuksanoh, H.Y. Yang, B.K. Chang, A.P. Queen, B.J. Tatarchuk, in: Y. Wang, J.D. Holladay (Eds.), ACS Symp. Series 914, Microreactor Technology and Process Intensification, Washington, DC, (2003), pp. 406–421.
[5] H.Y. Yang, Y. Lu, J. Bruce, Tatarchuk, J. Power Sources 174 (2007) 302–311.
[6] B.K. Chang, Y. Lu, H.Y. Yang, B.J. Tatarchuk, J. Mater. Eng. Perform. 15 (2006) 439–441.
[7] B.K. Chang, Y. Lu, B.J. Tatarchuk, Chem. Eng. J. 115 (2006) 195–202.
[8] B.K. Chang, Y. Lu, B.J. Tatarchuk, J. Mater. Eng. Perform. 15 (2006) 453–456.
[9] R.R. Kalluri, D.R. Cahela, B.J. Tatarchuk, Sep. Purif. Technol. 62 (2008) 304–316.
[10] A.P Queen, High Efficiency Adsorption Filters via Packed Bed + Polishing Sorbent Architectures for Regenerable Collective Protection Equipment, Masters Thesis, Auburn University, Auburn, AL, 2005.
[11] R.M. Heck, R.J. Farrauto, Catalytic Air Pollution Control: Commercial Technology, Van Nostrand Reinhold, New York, 1995.
[12] J.D. Spengler, S. Ludwig, R.A. Weker, Indoor Air 14 (2004) 67–73.
[13] National Research Council, The Airliner Cabin Environment and the Health of Passengers and Crew, National Academy Press, Washington, DC, 2002.
[14] E.H. Hunt, D.R. Space, The Airplane Cabin Environment-Issues Pertaining to Flight Attendant Comfort, International In-flight Service Management Organization Conference, Montreal, Canada, November, 1994.
[15] A. Torres, M.J. Utell, P.E. Morrow, Am. J. Respir. Crit. Care 156 (1997) 728–736.
[16] J. Lin, A. Kawai, T. Nakajima, Appl. Catal. B: Environ. 39 (2002) 157–165.
[17] B. Dhandapani, S.T. Oyama, Appl. Catal. B: Environ. 11 (1997) 129–166.
[18] R. Radhakrishnan, Structure and Ozone Decomposition Reactivity of Supported Manganese Oxide Catalysts, Ph.D. Thesis, Virginia Polytechnic Institute and State University, Blacksburg, VA, 2001.
[19] T. Kameya, K. Urano, J. Environ. Eng. 128 (2002) 286–292.
[20] R.C. Reid, J.M. Prausnitz, B.E. Poling, The Properties of Gases and Liquids, fourth ed., McGraw-Hill Book Company, New York, NY, 1987, pp. 587–588.
[21] H.S. Fogler, Elements of Reaction Engineering, third ed., Prentice Hall PTR, New Jersey, 1999.
[22] J.L. Williams, Catal. Today 69 (2001) 3–9.
[23] R.M. Heck, S. Gulati, R.J. Farrauto, Chem. Eng. J. 82 (2001) 149–156.
[24] R.M. Heck, R.J. Farrauto, H.C. Lee, Catal. Today 13 (1992) 43–58.
[25] E. Tronconi, A. Beretta, Catal. Today 52 (1991) 249–258.
[26] M. Uberoi, C.J. Pereire, Ind. Eng. Chem. Res. 35 (1996) 113–116.
[27] D.H. west, V. Balakotaiah, Z. Jovanovic, Catal. Today 88 (2003) 3–16.
[28] D.K. Harris, D.R. Cahela, B.J. Tatarchuk, Compos. Part A: Appl. Sci. 32 (2001) 1117–1126.
[29] D.R. Cahela, B.J. Tatarchuk, Catal. Today 69 (2001) 33–39.
[30] R.R. Kalluri, Microfibrous Entrapped Catalysts and Sorbents: Microstructured Heterogeneous Contacting Systems with Enhanced Efficiency, Ph.D. Dissertation, Auburn University, Auburn, AL, 2008.
[31] P.N. Dwivedi, S.N. Upadhyay, Ind. Eng. Chem., Process Des. Dev. 16 (1977) 157–165.
[32] A. Kołodziej, J. Łojewska, Chem. Eng. Process. 46 (2007) 637–648.
[33] L. Giani, G. Groppi, E. Tronconi, Ind. Eng. Chem. Res. 44 (2005) 4993–5002.
[34] F.C. Patcas, G.I. Garrido, B. Kraushaar-Czarnetzki, Chem. Eng. Sci. 62 (2007) 3984–3990.
[35] M.P. Galligan, J.C. Dettling, US Patent 5,422,331 (1995).
[36] W.F. Carr, M. Junction, H.M. Chen, US Patent 4,343,776 (1982).
[37] BASF DEOXO catalytic ozone converter–Product Information (http://www.catalysts.basf.com/Main/environmental/stationary_sources/indoor_air_quality/ozone_catalysts).
[38] V. Balakotaiah, D.H. West, Chem. Eng. Sci. 57 (2002) 1269–1286.